Available online at www.sciencedirect.com
SCIENCE DIRECT®
ELSEVIER
International Journal of Solids and Structures 43 (2006) 1276–1290
INTERNATIONAL JOURNAL OF SOLIDS and STRUCTURES
www.elsevier.com/locate/ijsolstr

Mechanical properties of single-walled carbon nanotubes based on higher order Cauchy–Born rule

X. Guo [a,b,*], J.B. Wang [a], H.W. Zhang [a,*]

[a] *Department of Engineering Mechanics, State Key Laboratory of Structural Analysis for Industrial Equipment, Dalian University of Technology, Dalian 116023, China*
[b] *Max-Planck Institute for Metals Research, Heisenbergstrasse 3, D-70569 Stuttgart, Germany*

Received 14 November 2004; received in revised form 26 May 2005
Available online 20 July 2005

Abstract

A nanoscale continuum theory is established based on the higher order Cauchy–Born rule to study the mechanical properties of carbon nanotubes. The theory bridges the microscopic and macroscopic length scale by incorporating the second-order deformation gradient into the kinematic description. Moreover, the interatomic potential and the atomic structure of carbon nanotube are incorporated into the proposed constitutive model in a consistent way. Therefore the single-walled carbon nanotube can be viewed as a macroscopic generalized continuum with microstructure. Based on the present theory, the energy and the size dependent mechanical properties of SWNT and graphite are predicted and compared with the existing experimental and theoretical data.

Keywords: Carbon nanotube; Cauchy–Born rule; Nanomechanics; Continuum mechanics

1. Introduction

Carbon nanotubes are tubular structures with nanometer diameter and micrometer length. Since the single-walled carbon nanotube (SWNT) and multi-walled carbon nanotube (MWNT) are found by Iijima (1991, 1993), there have been extensive researches on these nanomaterials. It has been found that carbon nanotubes possess many interesting and exceptional mechanical and electronic properties (Ruoff et al.,

* Corresponding authors. Tel.: +86 411 8470 7826; fax: +86 411 8470 8769.
E-mail addresses: guoxu@dlut.edu.cn, xu.guo@mf.mpg.de (X. Guo), zhanghw@dlut.edu.cn (H.W. Zhang).

0020-7683/$ - see front matter © 2005 Elsevier Ltd. All rights reserved.
doi:10.1016/j.ijsolstr.2005.05.049

2003; Popov, 2004). Therefore, it is expected that they can be used as promising materials for applications in nanoengineering. In order to make good use of these nanomaterials, it is important to have a good knowledge of their mechanical properties.

For the mechanical properties of carbon nanotubes, there have been numerous experiment studies. For example, Treacy et al. (1996) estimated that the Young's modulus of 11 MWNTs vary from 0.4 to 4.15 TPa with an average of 1.8 TPa by measuring the amplitude of their intrinsic thermal vibrations. Based on the experiment results, it is concluded that carbon nanotubes appear to be much stiffer than their graphite counterpart. With the use of the similar experiment method, Krishnan et al. (1998) reported that the Young's modulus is in the range of 0.9–1.70 TPa with an average of 1.25 TPa for 27 SWNTs. Direct tensile loading tests of SWNTs and MWNTs have also been performed by Yu et al. (2000a,b) and they reported that the Young's moduli are 0.32–1.47 TPa for SWNTs and 0.27–0.95 TPa for MWNTS, respectively. In the experiment, however, it is very difficult to measure the mechanical properties of carbon nanotubes directly due to their very small size.

There are also many research works using atomistic modeling approaches to investigate the mechanical properties of carbon nanotubes. Based on molecular dynamics simulation and Tersoff–Brenner atomic potential, Yakobson et al. (1996) predicted that the axial modulus of SWNTs are ranging from 1.4 to 5.5 TPa (note here that in their study, the wall thickness of SWNT was taken as 0.066 nm). By employing a non-orthogonal tight binding theory, Goze et al. (1999) investigated the Young's modulus of armchair and zigzag SWNTs with diameters of 0.5–2.0 nm. It was found that the Young's modulus is dependent on the diameter of the tube noticeably as the tube diameter is small. Popov et al. (2000) predicted the mechanical properties of SWNTs using Born's perturbation technique with a lattice-dynamical model. The results they obtained showed that the Young's modulus and the Poisson's ratio of both armchair and zigzag SWNTs depend on the tube radius as the tube radius are small. Other atomic modeling studies include first-principles based calculations (Zhou et al., 2001; Van Lier et al., 2000; Sánchez-Portal et al., 1999) and molecular dynamics simulations (Iijima et al., 1996). Although these atomic modeling techniques seem well suited to study problems related to molecular or atomic motions, these calculations are time-consuming and limited to systems with a small number of molecules or atoms.

Comparing with atomic modeling, continuum modeling is known to be more efficient from computational point of view. Therefore, many continuum modeling based approaches have been developed for study of carbon nanotubes. Based on Euler beam theory, Govindjee and Sackman (1999) studied the elastic properties of nanotubes and their size-dependent properties at nanoscale dimensions, which will not occur at continuum scale. Ru (2000a,b) proposed that the effective bending stiffness of SWNTs should be regarded as an independent material parameter. In his study of the stability of nanotubes under pressure, SWNT was treated as a single-layer elastic shell with effective bending stiffness. By equating the molecular potential energy of a nano-structured material with the strain energy of the representative truss and continuum models, Odega et al. (2002) studied the effective bending rigidity of a graphite sheet. Zhang et al. (2002a,b,c, 2004) proposed a nanoscale continuum theory for the study of SWNTs by directly incorporating the interatomic potentials into the constitutive model of SWNTs based on the modified Cauchy–Born rule. By employing this approach, the authors also studied the fracture nucleation phenomena in carbon nanotubes. Based on the work of Zhang et al. (2002c), Jiang et al. (2003) proposed an approach to account for the effect of nanotube radius on its mechanical properties. Chang and Gao (2003) studied the elastic modulus and Poisson's ratio of SWNTs by using molecular mechanics approach. In their work, analytical expressions for the mechanical properties of SWNT have been derived based on the atomic structure of SWNT. Li and Chou (2003) presented a structural mechanics approach to model the deformation of carbon nanotubes and obtained parameters by establishing a linkage between structural mechanics and molecular mechanics. Arroyo and Belytschko (2002a,b, 2004a,b) extended the standard Cauchy–Born rule and introduced the so-called exponential map to study the mechanical properties of SWNT since the classical Cauchy–Born rule cannot describe the deformation of crystalline film accurately. They also established

the numerical framework for the analysis of the finite deformation of carbon nanotubes. The results they obtained agree very well with those obtained by molecular mechanics simulations.

In the present paper, a nanoscale continuum theory is established based on the higher order Cauchy–Born rule to study the mechanical properties of carbon nanotubes. The theory bridges the microscopic and macroscopic length scale by incorporating the second-order deformation gradient into the kinematic description. Our idea is to use a higher-order Cauchy–Born rule to have a better description of the deformation of crystalline films with one or a few atom thickness with less computational efforts. Moreover, the interatomic potential and the atomic structure of carbon nanotube are incorporated into the proposed constitutive model in a consistent way. Therefore SWNT can be viewed as a macroscopic generalized continuum with microstructure. Based on the present theory, the energy and the size dependent mechanical properties of SWNT and graphite are predicted and compared with the existing experimental and theoretical data.

The paper is organized as follows: In Section 2, Tersoff–Brenner interatomic potential for carbon is introduced. In Sections 3 and 4, motivations for the introduction of the higher order Cauchy–Born rule are discussed. Section 5 gives the analytical expressions of the hyper-elastic constitutive model for SWNT based on the higher order Cauchy–Born rule. With the use of the proposed constitutive model, the mechanical properties (e.g. Young's modulus and Poisson's ratio) of SWNT are predicted in Section 6. Finally, some concluding remarks are given in Section 7.

2. The interatomic potential for carbon

In this section, Tersoff–Brenner interatomic potential for carbon (Tersoff, 1988; Brenner, 1990), which is widely used in the study of carbon nanotubes, is introduced as follows:

$$V(r_{IJ}) = V_R(r_{IJ}) - B_{IJ}V_A(r_{IJ}) \tag{1}$$

where

$$V_R(r) = f(r)\frac{D_e}{S-1}\mathrm{e}^{-\sqrt{2s}\beta(r-r_e)}, \quad V_A(r) = f(r)\frac{D_eS}{S-1}\mathrm{e}^{-\sqrt{2/s}\beta(r-r_e)} \tag{2}$$

$$f(r) = \begin{cases} 1 & r < r_1 \\ \frac{1}{2}\left\{1+\cos\left[\frac{\pi(r-r_1)}{(r_2-r_1)}\right]\right\} & r_1 \leqslant r \leqslant r_2 \\ 0 & r > r_2 \end{cases} \tag{3}$$

$$B_{IJ} = \left[1 + \sum_{K(\neq I,J)} G(\theta_{IJK})f(r_{IK})\right]^{-\delta} \tag{4}$$

$$G(\theta) = a_0\left[1 + \frac{c_0^2}{d_0^2} - \frac{c_0^2}{d_0^2 + (1+\cos\theta)^2}\right] \tag{5}$$

with the constants given in the following:

$$D_e = 6.000\ \mathrm{eV}, \quad S = 1.22, \quad \beta = 21\ \mathrm{nm}^{-1}, \quad r_e = 0.1390\ \mathrm{nm}$$
$$\delta = 0.50000, \quad a_0 = 0.00020813, \quad c_0 = 330, \quad d_0 = 3.5$$

Based on this set of parameters, the corresponding equilibrium bond length can be determined by

$$\frac{\partial V}{\partial r_{IJ}} = 0 \tag{6}$$

which is 0.145 nm for our case. This value is in good agreement with that of graphite (0.144 nm).

3. The limitation of the standard Cauchy–Born rule for crystal films

Cauchy–Born rule is a fundamental kinematic assumption for linking the deformation of the lattice vectors of crystal to that of a continuum deformation field. Without consideration of diffusion, phase transitions, lattice defect, slips or other non-homogeneities, it is very suitable for the linkage of 3D multiscale deformations of bulk materials such as space-filling crystals (Tadmor et al., 1996; Arroyo and Belytschko, 2002a,b, 2004a,b). In general, Cauchy–Born rule describes the deformation of the lattice vectors in the following way:

$$\boldsymbol{b} = \boldsymbol{F} \bullet \boldsymbol{a} \tag{7}$$

where $\boldsymbol{F}$ is the two-point deformation gradient tensor, $\boldsymbol{a}$ denotes the undeformed lattice vector and $\boldsymbol{b}$ represents the corresponding deformed lattice vector (see Fig. 1 for reference). In the deformed crystal, the length of the deformed lattice vector and the angle between two neighboring lattice vectors can be expressed by means of the standard continuum mechanics relations:

$$b = \sqrt{\boldsymbol{a} \bullet \boldsymbol{C}\boldsymbol{a}} \quad \text{and} \quad \cos\theta = \frac{\boldsymbol{a}' \bullet \boldsymbol{C}\boldsymbol{a}}{\|\boldsymbol{b}'\|\|\boldsymbol{b}\|} \tag{8}$$

where $\boldsymbol{b}' = \boldsymbol{F} \bullet \boldsymbol{a}'$ ($\boldsymbol{b}'$ and $\boldsymbol{a}'$ denote the neighboring deformed and undeformed lattice vector, respectively) and $\boldsymbol{C} = \boldsymbol{F}^{\mathrm{T}} \bullet \boldsymbol{F}$ is the Green strain tensor measured from undeformed configuration. θ represents the angle formed by the deformed lattice vectors $\boldsymbol{b}$ and $\boldsymbol{b}'$. Though the use of Cauchy–Born rule is suitable for bulk materials, as was first pointed out by Arroyo and Belytschko (2002a,b, 2004a,b), it is not suitable to apply it directly to the curved crystalline films with one or a few atoms thickness, especially when the curvature effects are dominated. One of the reasons is that if we view SWNT as a 2D manifold without thickness embedded in 3D Euclidean space, since the deformation gradient tensor $\boldsymbol{F}$ describes only the change of *infinitesimal* material vectors emanating from the same point in the tangent spaces of the undeformed and deformed curved manifolds (see Fig. 2 for an illustration), therefore the deformation gradient tensor $\boldsymbol{F}$ is not enough to give an accurate description of the length of the deformed lattice vector in the deformed configuration especially when the curvature of the film is relatively large. In this case, the standard Cauchy–Born rule should be modified to give a more accurate description for the deformation of curved crystalline films, such as carbon nanotubes.

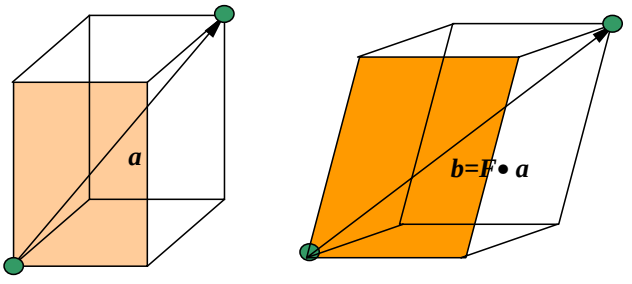

Fig. 1. Illustration of the Cauchy–Born rule.

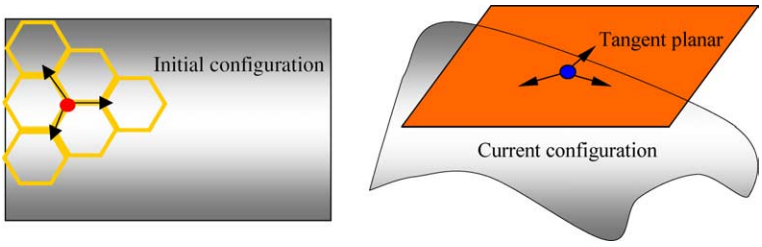

Fig. 2. The Cauchy–Born rule applied directly to curved films.

4. Higher order Cauchy–Born rule

In this section, an extension of the standard Cauchy–Born rule in order to alleviate its limitation for the description of the deformation of curved atom films is presented. To this end, we introduce the higher order deformation gradient into the kinematic relationship of SWNT. The same idea has also been shown by Leamy et al. (2003).

From the classical nonlinear continuum mechanics point of view, the deformation gradient tensor $\boldsymbol{F}$ is a linear transformation, which only describes the deformation of an *infinitesimal* material line element $\mathrm{d}\boldsymbol{X}$ in the undeformed configuration to an *infinitesimal* material line element $\mathrm{d}\boldsymbol{x}$ in deformed configuration, i.e.

$$\mathrm{d}\boldsymbol{x} = \boldsymbol{F} \bullet \mathrm{d}\boldsymbol{X} \tag{9}$$

As in Leamy et al. (2003), by taking the finite length of the initial lattice vector $\boldsymbol{a}$ into consideration, the corresponding deformed lattice vector should be expressed as

$$\boldsymbol{b} = \int_{\boldsymbol{0}}^{\boldsymbol{a}} \boldsymbol{F}(\boldsymbol{s})\,\mathrm{d}\boldsymbol{s} \tag{10}$$

Assuming that the deformation gradient tensor $\boldsymbol{F}$ is smooth enough, we can make a Taylor's expansion of the deformation field at $\boldsymbol{s} = \boldsymbol{0}$, which is corresponding to the starting point of the lattice vector $\boldsymbol{a}$.

$$\boldsymbol{F}(\boldsymbol{s}) = \boldsymbol{F}(\boldsymbol{0}) + \nabla\boldsymbol{F}(\boldsymbol{0}) \bullet \boldsymbol{s} + \nabla\nabla\boldsymbol{F}(\boldsymbol{0}) : (\boldsymbol{s}\otimes\boldsymbol{s})/2 + \mathbf{O}(\|\boldsymbol{s}\|^3) \tag{11}$$

Retaining up to the second order term of $\boldsymbol{s}$ in (11) and substituting it into (10), we can get the approximated deformed lattice vector as

$$\boldsymbol{b} \approx \boldsymbol{F}(\boldsymbol{0}) \bullet \boldsymbol{a} + \tfrac{1}{2}\nabla\boldsymbol{F}(\boldsymbol{0}) : (\boldsymbol{a}\otimes\boldsymbol{a}) \tag{12}$$

Comparing with the standard Cauchy–Born rule, it is obvious that with the use of this higher order term, we can pull the vector $\boldsymbol{F}\bullet\boldsymbol{a}$ more close to the deformed configuration (see Fig. 3 for an illustration). By retaining more higher-order terms, the accuracy of approximation can be enhanced. Comparing with the exponent Cauchy–Born rule proposed by Arroyo and Belytschko (2002a,b, 2004a,b), it can improve the standard Cauchy–Born rule for the description of the deformation of crystalline films with less computational effort.

It is worth noting that the dimension degeneration problem we wish to circumvent has its analogy in shell theory. The goal of the shell theory is to find an approximation of the three-dimensional linear elastic shell problem by a two-dimensional problem posed on the middle surface. This can always be accomplished by employing the technique of asymptotic energy analysis and theory of Γ-convergence. The same techniques can also be used in nanomechanics to develop the scheme for the passage from atomic to continuum theory for thin films, nanotubes and nanorods. On this aspect, we refer the readers to the paper of Friesecke and James (2000) and the references therein.

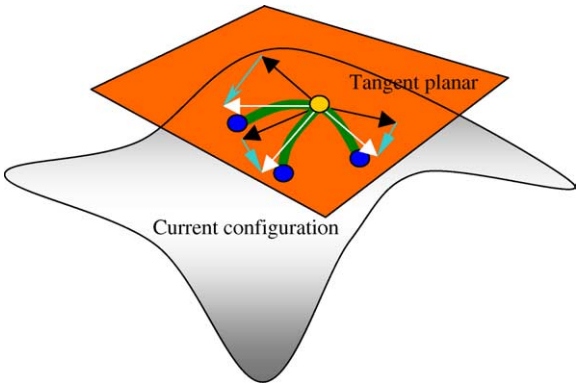

Fig. 3. Schematic illustration of the higher order Cauchy–Born rule.

5. The hyper-elastic constitutive model based on higher order Cauchy–Born rule

With the use of the above kinematic relation established by the proposed higher order Cauchy–Born rule, a constitutive model for SWNTs can be established. The key idea for continuum modeling of carbon nanotube is to relate the phenomenological macroscopic strain energy density W_0 per unit volume in the material configuration to the corresponding atomistic potential.

Assuming that the energy associated with an atom I can be homogenized over a representative volume V_I in the undeformed material configuration (i.e. graphite sheet, see Fig. 4 for reference), the strain energy density in this representative volume can be expressed as

$$W_0 = W_0(|\boldsymbol{r}_{I1}|, |\boldsymbol{r}_{I2}|, |\boldsymbol{r}_{I3}|) = \sum_{J=1}^{3} V_{IJ}(\boldsymbol{r}_{I1}, \boldsymbol{r}_{I2}, \boldsymbol{r}_{I3})/2V_I = W_0(\boldsymbol{F}, \boldsymbol{G}) \tag{13}$$

and

$$\boldsymbol{r}_{IJ} = \boldsymbol{F} \bullet \boldsymbol{R}_{IJ} + \boldsymbol{G} : (\boldsymbol{R}_{IJ} \otimes \boldsymbol{R}_{IJ})/2 \tag{14}$$

where $\boldsymbol{R}_{IJ}$ and $\boldsymbol{r}_{IJ}$ denote the undeformed and deformed lattice vectors, respectively. V_I is the volume of the representative cell. $\boldsymbol{F} = F_{ij}\boldsymbol{e}_i \otimes \boldsymbol{e}_j$ and $\boldsymbol{G} = \nabla \boldsymbol{F} = G_{ijk}\boldsymbol{e}_i \otimes \boldsymbol{e}_j \otimes \boldsymbol{e}_k$ are the first and second order deformation gradient tensors, respectively. Note that here and in the following discussions, a unified Cartesian coordinate

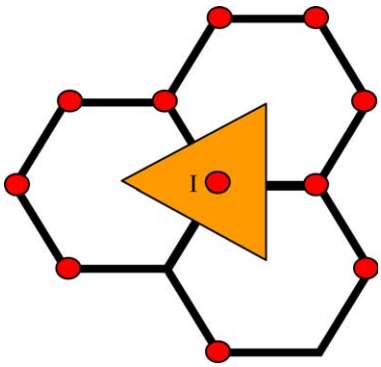

Fig. 4. Representative cell corresponding to an atom I.

system has been used for the description of the positions of material points in both of the initial and deformed configurations.

Based on the strain energy density W_0, as shown by Sunyk and Steinmann (2003), the first Piola–Kirchhoff stress tensor $\boldsymbol{P}$, which is work conjugate to $\boldsymbol{F}$ and the higher-order stress tensor $\boldsymbol{Q}$, which is work conjugate to $\boldsymbol{G}$ can be obtained as

$$\boldsymbol{P} = \frac{\partial W_0}{\partial \boldsymbol{F}} = \frac{1}{2V_I}\sum_{J=1}^{3} \boldsymbol{f}_{IJ} \otimes \boldsymbol{R}_{IJ} \tag{15}$$

$$\boldsymbol{Q} = \frac{\partial W_0}{\partial \boldsymbol{G}} = \frac{1}{4V_I}\sum_{J=1}^{3} \boldsymbol{f}_{IJ} \otimes \boldsymbol{R}_{IJ} \otimes \boldsymbol{R}_{IJ} \tag{16}$$

where $\boldsymbol{f}_{IJ}$ is the generalized force associated with the generalized coordinate $\boldsymbol{r}_{IJ}$, which is defined as

$$\boldsymbol{f}_{IJ} = \frac{\partial W}{\partial \boldsymbol{r}_{IJ}} \tag{17}$$

The corresponding strain energy density can also be rewritten as

$$W_0 = W/2V_I \tag{18}$$

where

$$W = \sum_{J=1}^{3} V_{IJ}(\boldsymbol{r}_{IJ}, \boldsymbol{r}_{IK}, \theta_{IJK},\ K \neq I, J) \tag{19}$$

denotes the total energy of the representative cell related to atom I caused by atomic interaction. V_{IJ} is the interatomic potential for carbon introduced in Section 2.

We can also define the generalized stiffness $\boldsymbol{K}_{IJIK}$ associated with the generalized coordinate $\boldsymbol{r}_{IJ}$ as

$$\boldsymbol{K}_{IJIK} = \frac{\partial \boldsymbol{f}_{IJ}}{\partial \boldsymbol{r}_{IK}} = \frac{\partial^2 W}{\partial \boldsymbol{r}_{IJ}\,\partial \boldsymbol{r}_{IK}} \tag{20}$$

where the subscripts I, J and K in the overstriking letters, such as $\boldsymbol{f}$, $\boldsymbol{r}$, $\boldsymbol{R}$ and $\boldsymbol{K}$, denote different atoms rather than the indices of the components of tensors. Therefore summation is not implied here by the repetition of these indices.

From (15) and (16), the tangent modulus tensors can be derived as

$$\boldsymbol{M}_{FF} = \frac{\partial^2 W_0}{\partial \boldsymbol{F} \otimes \partial \boldsymbol{F}} = \frac{1}{2V_I}\sum_{J=1}^{3}\sum_{K=1}^{3}[\boldsymbol{K}_{IJIK} \underline{\otimes} (\boldsymbol{R}_{IJ} \otimes \boldsymbol{R}_{IK})] \tag{21}$$

$$\boldsymbol{M}_{FG} = \frac{\partial^2 W_0}{\partial \boldsymbol{F} \otimes \partial \boldsymbol{G}} = \frac{1}{4V_I}\sum_{J=1}^{3}\sum_{K=1}^{3}[\boldsymbol{K}_{IJIK} \underline{\otimes} (\boldsymbol{R}_{IJ} \otimes \boldsymbol{R}_{IK})] \otimes \boldsymbol{R}_{IK} \tag{22}$$

$$\boldsymbol{M}_{GF} = \frac{\partial^2 W_0}{\partial \boldsymbol{G} \otimes \partial \boldsymbol{F}} = \frac{1}{4V_I}\sum_{J=1}^{3}\sum_{K=1}^{3}[\boldsymbol{K}_{IJIK} \overline{\otimes} (\boldsymbol{R}_{IJ} \otimes \boldsymbol{R}_{IJ})] \otimes \boldsymbol{R}_{IK} \tag{23}$$

$$\boldsymbol{M}_{GG} = \frac{\partial^2 W_0}{\partial \boldsymbol{G} \otimes \partial \boldsymbol{G}} = \frac{1}{8V_I}\sum_{J=1}^{3}\sum_{K=1}^{3}[\boldsymbol{K}_{IJIK} \overline{\otimes} (\boldsymbol{R}_{IJ} \otimes \boldsymbol{R}_{IJ})] \otimes (\boldsymbol{R}_{IK} \otimes \boldsymbol{R}_{IK}) \tag{24}$$

where $[\boldsymbol{A} \underline{\otimes} \mathbf{B}]_{ijkl} = A_{ik}B_{jl}$, $[\mathbf{A} \overline{\otimes} \mathbf{B}]_{ijkl} = A_{il}B_{jk}$. Compared with the results obtained by Zhang et al. (2002c), four tangent modulus tensors are presented here. This is due to the fact that second order deformation

gradient tensor has been introduced here for kinematic description. Therefore, from the macroscopic point of view, we can view the SWNT as a generalized continuum with microstructure.

Just as emphasized by Cousins (1978a,b), Tadmor et al. (1999), Zhang et al. (2002c) and Arroyo and Belytschko (2002a), since the atomic structure of carbon nanotube is not centrosymmetric, the standard Cauchy–Born rule can not be used directly since it cannot guarantee the inner equilibrium of the representative cell. An inner shift vector $\boldsymbol{\eta}$ must be introduced to achieve this goal. The inner shift vector can be obtained by minimizing the strain energy density of the unit cell with respect to $\boldsymbol{\eta}$

$$\hat{\boldsymbol{\eta}}(\boldsymbol{F},\boldsymbol{G}) = \arg\left(\min_{\boldsymbol{\eta}} W_0(\boldsymbol{F},\boldsymbol{G},\boldsymbol{\eta})\right) \Rightarrow \left.\frac{\partial W_0}{\partial \boldsymbol{\eta}}\right|_{\boldsymbol{\eta}=\hat{\boldsymbol{\eta}}} = \boldsymbol{0} \tag{25}$$

Substituting (25) into $W_0(\boldsymbol{F},\boldsymbol{G},\boldsymbol{\eta})$, we have

$$\hat{W}_0(\boldsymbol{F},\boldsymbol{G}) = W_0(\boldsymbol{F},\boldsymbol{G},\hat{\boldsymbol{\eta}}(\boldsymbol{F},\boldsymbol{G})) \tag{26}$$

Then the modified tangent modulus tensors can be obtained as

$$\hat{\boldsymbol{M}}_{FF} = \frac{\partial^2 \hat{W}_0}{\partial \boldsymbol{F}\otimes\partial \boldsymbol{F}} = \boldsymbol{M}_{FF}|_{\boldsymbol{\eta}=\hat{\eta}} - \left.\left[\frac{\partial^2 W_0}{\partial \boldsymbol{F}\otimes\partial\boldsymbol{\eta}}\left(\frac{\partial^2 W_0}{\partial\boldsymbol{\eta}\otimes\partial\boldsymbol{\eta}}\right)^{-1}\frac{\partial^2 W_0}{\partial\boldsymbol{\eta}\otimes\partial\boldsymbol{F}}\right]\right|_{\boldsymbol{\eta}=\hat{\boldsymbol{\eta}}} \tag{27}$$

$$\hat{\boldsymbol{M}}_{FG} = \frac{\partial^2 \hat{W}_0}{\partial \boldsymbol{F}\otimes\partial \boldsymbol{G}} = \boldsymbol{M}_{FG}|_{\boldsymbol{\eta}=\hat{\boldsymbol{\eta}}} - \left.\left[\frac{\partial^2 W_0}{\partial \boldsymbol{F}\otimes\partial\boldsymbol{\eta}}\left(\frac{\partial^2 W_0}{\partial\boldsymbol{\eta}\otimes\partial\boldsymbol{\eta}}\right)^{-1}\frac{\partial^2 W_0}{\partial\boldsymbol{\eta}\otimes\partial\boldsymbol{G}}\right]\right|_{\boldsymbol{\eta}=\hat{\boldsymbol{\eta}}} \tag{28}$$

$$\hat{\boldsymbol{M}}_{GF} = \frac{\partial^2 \hat{W}_0}{\partial \boldsymbol{G}\otimes\partial \boldsymbol{F}} = \boldsymbol{M}_{GF}|_{\boldsymbol{\eta}=\hat{\boldsymbol{\eta}}} - \left.\left[\frac{\partial^2 W_0}{\partial \boldsymbol{G}\otimes\partial\boldsymbol{\eta}}\left(\frac{\partial^2 W_0}{\partial\boldsymbol{\eta}\otimes\partial\boldsymbol{\eta}}\right)^{-1}\frac{\partial^2 W_0}{\partial\boldsymbol{\eta}\otimes\partial\boldsymbol{F}}\right]\right|_{\boldsymbol{\eta}=\hat{\boldsymbol{\eta}}} \tag{29}$$

$$\hat{\boldsymbol{M}}_{GG} = \frac{\partial^2 \hat{W}_0}{\partial \boldsymbol{G}\otimes\partial \boldsymbol{G}} = \boldsymbol{M}_{GG}|_{\boldsymbol{\eta}=\hat{\boldsymbol{\eta}}} - \left.\left[\frac{\partial^2 W_0}{\partial \boldsymbol{G}\otimes\partial\boldsymbol{\eta}}\left(\frac{\partial^2 W_0}{\partial\boldsymbol{\eta}\otimes\partial\boldsymbol{\eta}}\right)^{-1}\frac{\partial^2 W_0}{\partial\boldsymbol{\eta}\otimes\partial\boldsymbol{G}}\right]\right|_{\boldsymbol{\eta}=\hat{\boldsymbol{\eta}}} \tag{30}$$

where

$$\boldsymbol{M}_{FF}|_{\eta=\hat{\eta}} = \frac{1}{2V_I}\sum_{J=1}^{3}\sum_{K=1}^{3}[\hat{\boldsymbol{K}}_{IJIK} \underline{\otimes} ((\boldsymbol{R}_{IJ}+\hat{\eta})\otimes(\boldsymbol{R}_{IJ}+\hat{\eta}))] \tag{31a}$$

$$\boldsymbol{M}_{FG}|_{\boldsymbol{\eta}=\hat{\boldsymbol{\eta}}} = \frac{1}{4V_I}\sum_{J=1}^{3}\sum_{K=1}^{3}[\hat{\boldsymbol{K}}_{IJIK} \underline{\otimes} ((\boldsymbol{R}_{IJ}+\hat{\boldsymbol{\eta}})\otimes(\boldsymbol{R}_{IK}+\hat{\boldsymbol{\eta}}))]\otimes(\boldsymbol{R}_{IK}+\hat{\boldsymbol{\eta}}) \tag{31b}$$

$$M_{GF}|_{\eta=\hat{\eta}} = \frac{1}{4V_I}\sum_{J=1}^{3}\sum_{K=1}^{3}[\hat{\boldsymbol{K}}_{IJIK} \overline{\otimes} ((\boldsymbol{R}_{IJ}+\hat{\boldsymbol{\eta}})\otimes(\boldsymbol{R}_{IJ}+\hat{\boldsymbol{\eta}}))]\otimes(\boldsymbol{R}_{IK}+\hat{\boldsymbol{\eta}}) \tag{31c}$$

$$\boldsymbol{M}_{GG}|_{\eta=\hat{\eta}} = \frac{1}{8V_I}\sum_{J=1}^{3}\sum_{K=1}^{3}[\hat{\boldsymbol{K}}_{IJIK} \overline{\otimes} ((\boldsymbol{R}_{IJ}+\hat{\boldsymbol{\eta}})\otimes(\boldsymbol{R}_{IJ}+\hat{\boldsymbol{\eta}}))]\otimes((\boldsymbol{R}_{IK}+\hat{\boldsymbol{\eta}})\otimes(\boldsymbol{R}_{IK}+\hat{\boldsymbol{\eta}})) \tag{31d}$$

$$\hat{\boldsymbol{K}}_{IJIK} = \left.\frac{\partial^2 W}{\partial \boldsymbol{r}_{IJ}\otimes\partial\boldsymbol{r}_{IJ}}\right|_{\boldsymbol{\eta}=\hat{\boldsymbol{\eta}},\boldsymbol{r}_{IJ}=\hat{\boldsymbol{r}}_{IJ}} \tag{32}$$

$$\hat{\boldsymbol{r}}_{IJ} = \boldsymbol{F}\bullet(\boldsymbol{R}_{IJ}+\hat{\boldsymbol{\eta}}) + \boldsymbol{G}:[(\boldsymbol{R}_{IJ}+\hat{\boldsymbol{\eta}})\otimes(\boldsymbol{R}_{IJ}+\hat{\boldsymbol{\eta}})]/2 \tag{33}$$

$$\left.\frac{\partial^2 W_0}{\partial \boldsymbol{F}\otimes\partial\boldsymbol{\eta}}\right|_{\boldsymbol{\eta}=\hat{\boldsymbol{\eta}}} = \frac{1}{2V_I}\sum_{J=1}^{3}\left[\sum_{K=1}^{3}\left((\hat{\boldsymbol{K}}_{IJIK}\bullet\boldsymbol{F})\dot{\otimes}(\boldsymbol{R}_{IJ}+\hat{\boldsymbol{\eta}}) + \dot{\mathrm{sym}}(\hat{\boldsymbol{K}}_{IJIK}\bullet\mathbf{G}\right.\right.$$
$$\left.\left.\bullet((\boldsymbol{R}_{IK}+\hat{\boldsymbol{\eta}})\otimes(\boldsymbol{R}_{IJ}+\hat{\boldsymbol{\eta}}))\right) + \hat{\boldsymbol{f}}_{IJ}\otimes^2\mathbf{1}\right] \tag{34}$$

$$\left.\frac{\partial W_0}{\partial \boldsymbol{\eta}}\right|_{\boldsymbol{\eta}=\hat{\boldsymbol{\eta}}} = \frac{1}{2V_I}\sum_{J=1}^{3}\hat{\boldsymbol{f}}_{IJ} \bullet [\boldsymbol{F} + \underset{\bullet}{\mathrm{sym}}(\boldsymbol{G} \bullet (\boldsymbol{R}_{IJ} + \hat{\boldsymbol{\eta}}))] \tag{35}$$

$$\left.\frac{\partial^2 W_0}{\partial \boldsymbol{\eta} \otimes \partial \boldsymbol{F}}\right|_{\boldsymbol{\eta}=\hat{\boldsymbol{\eta}}} = \frac{1}{2V_I}\sum_{J=1}^{3}\left[\sum_{K=1}^{3}\left((\boldsymbol{F} + \underset{\bullet}{\mathrm{sym}}(\boldsymbol{G} \bullet (\boldsymbol{R}_{IJ} + \hat{\boldsymbol{\eta}})))^{\boldsymbol{T}} \bullet (\hat{\boldsymbol{K}}_{IJIK} \otimes (\boldsymbol{R}_{IK} + \hat{\boldsymbol{\eta}}))\right) + \hat{\boldsymbol{f}}_{IJ} \underset{\bullet}{\otimes}^2 \mathbf{1}\right] \tag{36}$$

$$\left.\frac{\partial^2 W_0}{\partial \boldsymbol{\eta} \otimes \partial \boldsymbol{\eta}}\right|_{\boldsymbol{\eta}=\hat{\boldsymbol{\eta}}} = \frac{1}{2V_I}\sum_{J=1}^{3}\left[\sum_{K=1}^{3}(\boldsymbol{F} + \underset{\bullet}{\mathrm{sym}}(\boldsymbol{G} \bullet (\boldsymbol{R}_{IJ} + \hat{\boldsymbol{\eta}})))^{\boldsymbol{T}} \bullet \hat{\boldsymbol{K}}_{IJIK} \bullet (\boldsymbol{F} + \underset{\bullet}{\mathrm{sym}}(\boldsymbol{G} \bullet (\boldsymbol{R}_{IK} + \hat{\boldsymbol{\eta}}))) + \hat{\boldsymbol{f}}_{IJ} \bullet \underset{\bullet}{\mathrm{sym}}\,\boldsymbol{G}\right] \tag{37}$$

$$\left.\frac{\partial^2 W_0}{\partial \boldsymbol{G} \otimes \partial \boldsymbol{\eta}}\right|_{\boldsymbol{\eta}=\hat{\boldsymbol{\eta}}} = \frac{1}{4V_I}\sum_{J=1}^{3}\left[\sum_{K=1}^{3}(\underset{\bullet}{\mathrm{sym}}(\hat{\boldsymbol{K}}_{IJIK} \bullet \boldsymbol{G} \bullet ((\boldsymbol{R}_{IK} + \hat{\boldsymbol{\eta}}) \otimes (\boldsymbol{R}_{IJ} + \hat{\boldsymbol{\eta}}) \otimes (\boldsymbol{R}_{IJ} + \hat{\boldsymbol{\eta}}))) + (\hat{\boldsymbol{K}}_{IJIK} \bullet \boldsymbol{F}) \underset{\bullet}{\otimes} (\boldsymbol{R}_{IK} + \hat{\boldsymbol{\eta}}) \underset{\bullet}{\otimes} (\boldsymbol{R}_{IK} + \hat{\boldsymbol{\eta}})) + (\hat{\boldsymbol{f}}_{IJ} \overline{\otimes} (\boldsymbol{R}_{IJ} + \hat{\boldsymbol{\eta}}) \overline{\otimes}^2 \mathbf{1}) + (\hat{\boldsymbol{f}}_{IJ} \otimes (\boldsymbol{R}_{IJ} + \hat{\boldsymbol{\eta}}) \otimes^2 \mathbf{1})\right] \tag{38}$$

$$\left.\frac{\partial^2 W_0}{\partial \boldsymbol{\eta} \otimes \partial \boldsymbol{G}}\right|_{\boldsymbol{\eta}=\hat{\boldsymbol{\eta}}} = \frac{1}{2V_I}\sum_{J=1}^{3}\left[\sum_{K=1}^{3}\left(\frac{1}{2}\left((\boldsymbol{F} + \underset{\bullet}{\mathrm{sym}}(\boldsymbol{G} \bullet (\boldsymbol{R}_{IJ} + \hat{\boldsymbol{\eta}})))^{\boldsymbol{T}} \bullet (\hat{\boldsymbol{K}}_{IJIK} \otimes (\boldsymbol{R}_{IK} + \hat{\boldsymbol{\eta}}) \otimes (\boldsymbol{R}_{IK} + \hat{\boldsymbol{\eta}}))\right)\right) + \underset{\bullet}{\mathrm{sym}}(\hat{\boldsymbol{f}}_{IJ} \otimes^2 \mathbf{1} \otimes (\boldsymbol{R}_{IJ} + \hat{\boldsymbol{\eta}}))\right] \tag{39}$$

where $^2\mathbf{1}$ is the second order identity tensor. The symbols used in the above expressions are defined as

$$\left(\underset{\bullet}{\mathrm{sym}}[\boldsymbol{A} \bullet \boldsymbol{B} \bullet (\boldsymbol{c} \otimes \boldsymbol{d})]\right)_{ijk} = (A_{ip}B_{pkn}c_n d_j + A_{ip}B_{pqk}c_q d_j)/2 \tag{40}$$

$$\left(\boldsymbol{A} \underset{\bullet}{\otimes} \boldsymbol{b}\right)_{ijk} = A_{ik}b_j \tag{41}$$

$$\left[\underset{\bullet}{\mathrm{sym}}(\boldsymbol{B} \bullet \boldsymbol{b})\right]_{ij} = (B_{ijr}b_r + B_{irj}b_r)/2 \tag{42}$$

$$\left(\boldsymbol{a} \underset{\bullet}{\otimes} \boldsymbol{A}\right)_{ijk} = a_j A_{ik} \tag{43}$$

$$\left(\underset{\bullet}{\mathrm{sym}}\,\boldsymbol{G}\right)_{ijk} = (G_{ijk} + G_{ikj})/2 \tag{44}$$

$$[(\boldsymbol{a} \overline{\otimes} \boldsymbol{b}) \overline{\otimes} \boldsymbol{A}]_{ijkl} = a_i b_k A_{jl} \tag{45}$$

$$\left(\underset{\bullet}{\mathrm{sym}}[\boldsymbol{A} \bullet \boldsymbol{B} \bullet (\boldsymbol{c} \otimes \boldsymbol{d} \otimes \boldsymbol{d})]\right)_{ijkl} = (A_{ip}B_{plr}c_r d_j d_k + A_{ip}B_{pql}c_q d_j d_k)/2 \tag{46}$$

$$\left(\boldsymbol{A} \underset{\bullet}{\otimes} \boldsymbol{c} \underset{\bullet}{\otimes} \boldsymbol{c}\right)_{ijkl} = A_{il}c_j c_k \tag{47}$$

$$\left(\overset{\bullet}{\underset{\bullet}{\mathrm{sym}}}(\boldsymbol{a}\otimes\boldsymbol{A}\otimes\boldsymbol{b})\right)_{ijkl} = (a_jA_{ik}b_l + a_jA_{il}b_k)/2 \tag{48}$$

6. Size-dependent mechanical properties of SWNTs

Based on the above explicit expressions of the constitutive tensors, we can calculate the strain energy per atom and predict the size-dependent mechanical properties of SWNTs.

It is usually thought that SWNTs can be formed by rolling a graphite sheet into a hollow cylinder as shown in Fig. 5. In the present calculation, a planar graphite sheet in equilibrium energy state is defined as the undeformed configuration. The current configuration of the nanotube can be seen as deformed from the initial configuration by the following mapping:

$$x_1 = X_1, \quad x_2 = R\sin\frac{X_2}{R}, \quad x_3 = R\cos\frac{X_2}{R} - R \tag{49}$$

where (X_1, X_2) are the material coordinates of a point in the undeformed configuration and (x_1, x_2, x_3) are its images in the current configuration. R is the radius of the modeled SWNT, which is described by a pair of parameters (n, m). The radius R can be evaluated by $R = a\sqrt{m^2 + mn + n^2}/2\pi$ with $a = a_0\sqrt{3}$, where a_0 is the equilibrium bond length of the atoms in the graphite sheet.

6.1. The energy per atom for SWNTs and graphite

First, based on the present model, the energy per atom of the graphite sheet is calculated and the value of -1.1801 Kg nm^2/s^2 is obtained. It can be found that the present value agrees well with that of -7.3756 eV (1 eV $= 1.6\times10^{-19}$ Nm) given by Robertson et al. (1992) with the use of the same interatomic potential.

The energy per atom as the function of diameters for armchair and zigzag SWNTs relative to that of the graphite sheet is also calculated. It is shown in Fig. 6 that the trend is almost the same for both armchair and zigzag SWNTs. The energy per atom decreases with increase of the tube diameter with $E(D) - E(\infty) = \mathrm{O}(1/D^2)$, where $E(\infty)$ represents the energy per atom for graphite sheet.

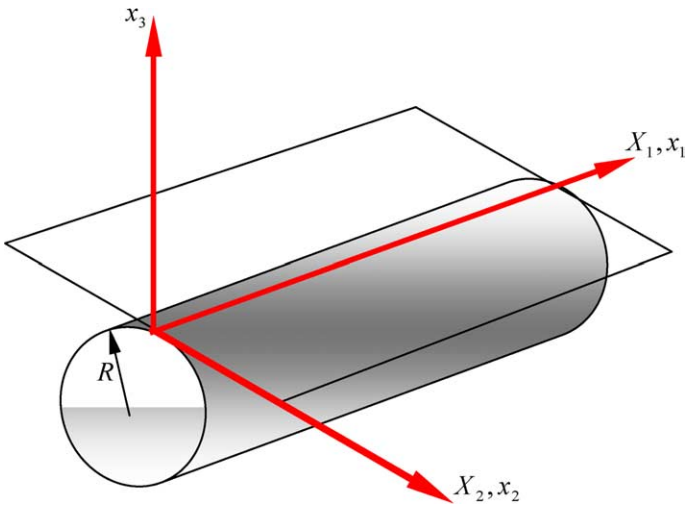

Fig. 5. Schematic illustration of rolling a graphite sheet into SWNT.

For larger tube diameter, the energy per atom approaches that of graphite. On the whole, it can be shown that the energy per atom depends obviously on tube diameters, but does not depend on tube chirality. For comparison, the results obtained by Robertson et al. (1992) with the use of both empirical potential and first-principle method based on the same interatomic potential are also shown in Fig. 6. It can be found that the present results are not only in good agreement with Robertson's results, but also with those obtained by Jiang et al. (2003) based on incorporating the interatomic potential (Tersoff–Brenner potential) into the continuum analysis.

6.2. The elastic properties of SWNTs and graphite

In this section, we will discuss the size-dependent mechanical properties of SWNTs. As shown by Zhang et al. (2002c), the Young's modulus and the Poisson's ratio of planar graphite can be obtained from $\hat{\boldsymbol{M}}_{FF}$ by the following expressions:

$$E = (\hat{\boldsymbol{M}}_{FF})_{1111} - \frac{(\hat{\boldsymbol{M}}_{FF})_{1122}^2}{(\hat{\boldsymbol{M}}_{FF})_{2222}} \tag{50}$$

$$v = \frac{(\hat{\boldsymbol{M}}_{FF})_{1122}}{(\hat{\boldsymbol{M}}_{FF})_{1111}} \tag{51}$$

For curved graphites (SWNTs), we also use the above expressions to estimate their mechanical properties along the axial direction although the corresponding elasticity tensors are no longer isotropic as in planar graphite case. Note that all calculations performed here are based on the Cartesian coordinate system and the Young's modulus E is obtained by dividing the thickness of the wall of SWNT, which is often taken as 0.334 nm in the literature.

To illustrate the validity of the analytical formulations obtained in the preceding sections, the prediction of the mechanical properties of graphite and SWNTs has been carried out based on Tersoff–Brenner potential. The relevant numerical results are shown in Fig. 7.

As for the graphite, The resulting Young's modulus is 0.69 TPa (see the dashed line in Fig. 7(a)), which agrees well with that suggested by Zhang et al. (2002c) and Arroyo and Belytschko (2004b) based on the same interatomic potential (represents by the horizontal solid line in Fig. 6(a)). The Poisson's ratio

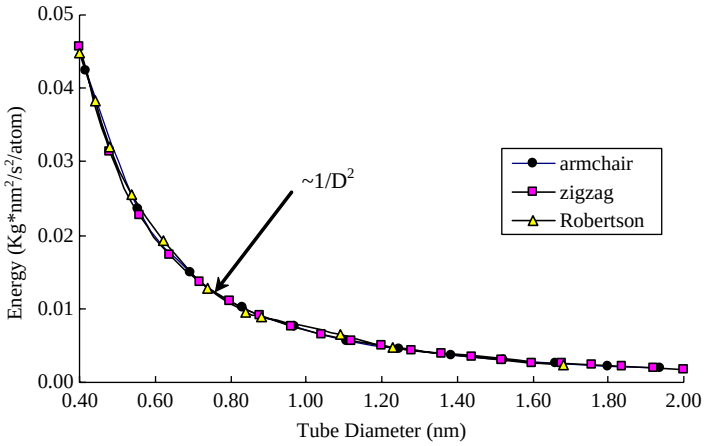

Fig. 6. The energy (relative to graphite) per atom versus tube diameter.

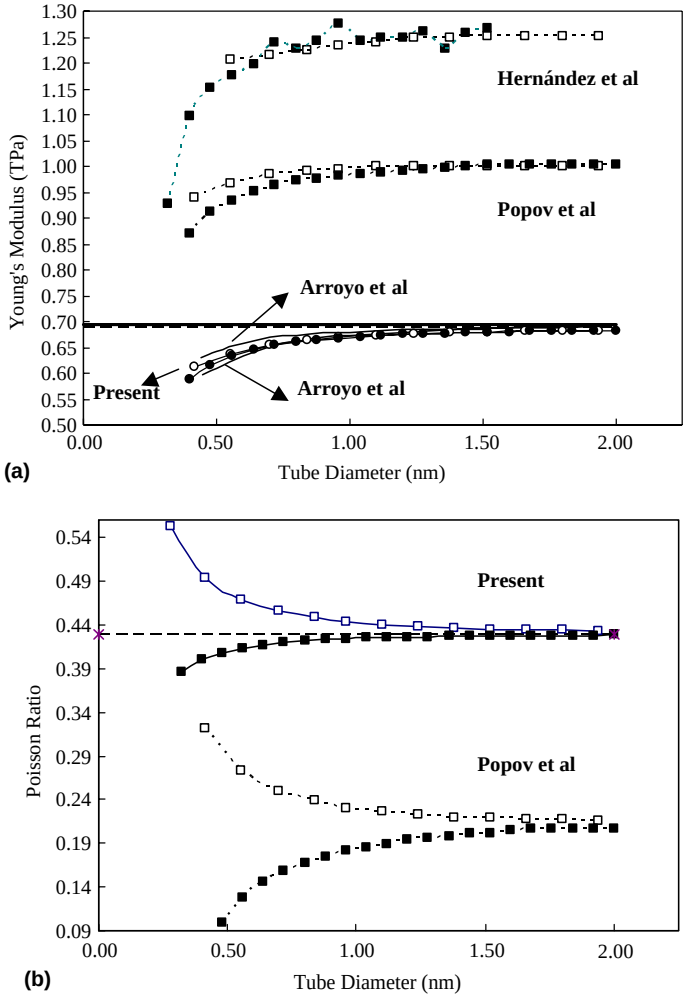

Fig. 7. Comparison between the results obtained with different methods (a) Young's modulus and (b) Poisson's ratio. Open symbols denote armchair, solid symbols denote zigzag. Dashed horizontal line denotes the results of graphite obtained with the present approach and the solid horizontal line denotes the results of graphite obtained by Arroyo and Belytschko (2004b) with exponential mapping, respectively.

predicted by the present approach is 0.4295 (see the dashed line shown in Fig. 7(b)), which is also very close to the value of 0.4123 given by Arroyo and Belytschko (2004b) using the same interatomic potential.

It is worth noting that the inner displacement has a significant influence on the Young's modulus and the Poisson's ratio of graphite. If no inner relaxation is taken into consideration (i.e. omitting the second term in the right hand side of (27)), the corresponding Young's modulus is 1.01 TPa and the Poisson's ratio is 0.16, which also agree well with the corresponding non-relaxation results obtained by Arroyo and Belytschko (2004b). As pointed out by Arroyo and Belytschko (2004b), although these values are close to the accurate ab initio data (Kudin et al., 2001), they do not represent the actual behavior of atomistic systems described by Brenner's potential.

As for SWNTs, Fig. 7(a) displays the variations of the Young's modulus with different diameters and chiralities. It can be observed that the trend is similar for both armchair and zigzag SWNTs and the

influence of nanotube chirality is not significant. For smaller tubes whose diameters are less than 1.3 nm, the Young's modulus strongly depends on the tube diameter. However, for tubes diameters larger than 1.3 nm, the dependence becomes very weak. As a whole, it can be seen that for both armchair and zigzag SWNTs the Young's modulus increases with increase of tube diameter and a plateau is reached when the diameter is large, which corresponds to the modulus of graphite predicted by the present method. The existing non-orthogonal tight binding results given by Hernández et al. (1998), lattice-dynamics results given by Popov et al. (2000) and the exponential Cauchy–Born rule based results given by Arroyo and Belytschko (2002b) are also shown in Fig. 7(a) for comparison. Comparing with the results given by Hernández et al. (1998) and Popov et al. (2000), it can be seen that although their data are larger than the corresponding ones of the present model, the general tendencies predicted by different methods are in good agreement. From the trend to view, the present predicted trend is also in reasonable agreement with that given by Robertson et al. (1992), Arroyo and Belytschko (2002b), Chang and Gao (2003) and Jiang et al. (2003). As for the differences between the values of different methods, it may be due to the fact that different parameters and atomic potential are used in different theories or algorithms (Chang and Gao, 2003). For example, Yakobson et al. (1996) result of surface Young's modulus of carbon nanotube based on molecular dynamics simulation with Tersoff–Brenner potential is about 0.36 TPa nm, while Overney et al. (1993) result based on Keating potential is about 0.51 TPa nm. Recent ab initio calculations by Sánchez-Portal et al. (1999) and Van Lier et al. (2000) showed that Young's modulus of SWNTs may vary from 0.33 to 0.37 TPa nm and from 0.24 to 0.40 TPa nm, respectively. Furthermore, it can be found that our computational results agree well with that given by Arroyo and Belytschko (2002b) with their exponential Cauchy–Born rule. They are also in reasonable agreement with the experimental results of 0.8 ± 0.4 TPa given by Salvetat et al. (1999).

From Fig. 7(b), the effect of tube diameter on the Poisson's ratio is also clearly observed. It can be seen that, for both armchair and zigzag SWNTs, the Poisson's ratio is very sensitive to the tube diameters especially when the diameter is less than 1.3 nm. The Poisson's ratio of armchair nanotube decreases with increasing tube diameter but the situation is opposite for that of the zigzag one. However, as the tube diameters are larger than 1.3 nm, the Poisson's ratio of both armchair and zigzag SWNTs reach a limit value i.e. the Poisson's ratio of the planar graphite. For comparison, the corresponding results suggested by Popov et al. (2000) are also shown in Fig. 7(b). It can be observed that the tendencies are very similar between the results given by Popov et al. (2000) and the present method although the values are different. Moreover, it is worth noting although many investigations on the Poisson's ratio of SWNTs have been conducted, there is no unique opinion that is widely accepted. For instance, Goze et al. (1999) showed that the Poisson's ratio of $(10,0)$, $(20,0)$, $(10,0)$ and $(20,0)$ tubes are 0.275, 0.270, 0.247 and 0.256, respectively. Based on a molecular mechanics approach, Chang and Gao (2003) suggested that the Poisson's ratio for armchair and zigzag SWNTs will decrease with increase of tube diameters from 0.19 to 0.16, and 0.26 to 0.16, respectively. In recent ab initio studies of Van Lier et al. (2000), even negative Poisson's ratio is reported.

It also can be seen from Fig. 7(b) that the obtained Poisson's ratio is a little bit high when tube diameter is less than 0.3 nm. It may be ascribed to the fact that when tube diameter is less than 0.3 nm, because of the higher value of curvature, higher order ($\geqslant 2$) deformation gradient tensor should be taken into account in order to describe the deformation of the atomic bonds more accurately. Another possible explanation is that for such small values of diameter, more accurate interatomic potential should be used in this extreme case.

7. Concluding remarks

In the present paper, a higher order Cauchy–Born rule has been adopted for the modeling of carbon nanotubes. In the present model, by including the second order deformation gradient tensor in the kinematic description, we can alleviate the limitation of the standard Cauchy–Born rule for the modeling of

nanoscale crystalline films with less computational efforts. Based on the established relationship between the atomic potential and the macroscopic continuum strain energy, analytical expressions for the tangent modulus tensors are derived. From these expressions, the hyper-elastic constitutive law for this generalized continuum can be obtained. With the use of this approach and the Tersoff–Brenner atomic potential for carbon, the size dependent mechanical properties of carbon nanotube are predicted. The obtained results agree well with those obtained by other experimental, atomic modeling and continuum concept based studies.

It should be pointed out that the present method is not limited to a specific interatomic potential and the study of SWNTs. It can also be applied to calculate the mechanical response of MWNTs. The proposed model can be further applied to other nano-film materials, such as BN and BC_3 nanotubes. The key point is to view them as generalized continuum with microstructures.

Acknowledgements

This work is supported by the *China Natural Science Foundation* under the grants of no. 10225212, no. 10472022; the Program for Changjiang Scholars and NCET Program provided by the Ministry of Education of China and the support of Max-Planck Society of Germany. The first author also acknowledges the fruitful discussions with Prof. Gao Hua Jian in Max-Planck Institute for Metals Research.

References

Arroyo, M., Belytschko, T., 2002a. An atomistic-based finite deformation membrane for single layer crystalline films. Journal of the Mechanics and Physics of Solids 50, 1941–1977.

Arroyo, M., Belytschko, T., 2002b. Large deformation atomistic-based continuum analysis of carbon nanotubes. American Institute of Aeronautics and Astronautics, 1–10.

Arroyo, M., Belytschko, T., 2004a. Finite element methods for the non-linear mechanics of crystalline sheets and nanotubes. International Journal for Numerical Methods in Engineering 59, 419–456.

Arroyo, M., Belytschko, T., 2004b. Finite crystal elasticity of carbon nanotubes based on the exponential Cauchy–Born rule. Physical Review B 69, 115415-1–115415-11.

Brenner, D.W., 1990. Empirical potential for hydrocarbons for use in simulation the chemical vapor deposition of diamond films. Physical Review B 42, 9458–9471.

Chang, T.C., Gao, H.J., 2003. Size-dependent elastic properties of a single-walled carbon nanotube via a molecular mechanics model. Journal of the Mechanics and Physics of Solids 51, 1059–1074.

Cousins, C.S.G., 1978a. Inner elasticity. Journal of Physics C: Solid State Physics 11, 4867–4879.

Cousins, C.S.G., 1978b. The symmetry of inner elastic constants. Journal of Physics C: Solid State Physics 11, 4881–4900.

Friesecke, G., James, R.D., 2000. A scheme for the passage from atomic to continuum therapy for thin films, nanotubes and nanorods. Journal of the Mechanics and Physics of Solids 48, 1519–1540.

Govindjee, S., Sackman, J.L., 1999. On the use of continuum mechanics to estimate the properties of nanotubes. Solid State Communication 110, 227–230.

Goze, C., Vaccarini, L., Henrard, L., Bernier, P., Hernández, E., Rubio, A., 1999. Elastic and mechanical properties of carbon nanotubes. Synthetic Metals 103, 2500–2501.

Hernández, E., Goze, C., Bernier, P., Rubio, A., 1998. Elastic properties of C and B_xC_y Nz composite nanotubes. Physical Review Letters 80, 4502–4505.

Iijima, S., 1991. Helical microtubules of graphitic carbon. Nature 354, 56–58.

Iijima, S., Ichlhashi, T., 1993. Single-shell carbon nanotubes of 1-nm diameter. Nature 363, 603–605.

Iijima, S., Brabec, C., Maiti, A., Bernholc, J., 1996. Structural flexibility of carbon nanotubes. Journal of Chemical Physics 104, 2089–2092.

Jiang, H., Zhang, P., Liu, B., Huang, Y., Geubelle, P.H., Gao, H., Hwang, K.C., 2003. The effect of nanotube radius on the constitutive model for carbon nanotubes. Computational Materials Science 28, 429–442.

Krishnan, A., Dujardin, E., Ebbesen, T.W., Yianilos, P.N., Treacy, M.M.J., 1998. Young's modulus of single-walled nanotubes. Physical Review B 58, 14013–14019.

Kudin, D., Scuseria, G., Yakobson, B., 2001. C_2, BN, and C nanoshell elasticity from ab initio computations. Physical Review B 64, 235406.

Leamy, M.J., Chung, P.W., Namburu, R., 2003. On an exact mapping and a higher-order Born rule for use in analyzing graphene carbon nanotubes. In: Proceedings of the 11th Annual ARL-USMA Technical Symposium, November 5.

Li, Ch.Y., Chou, T.W., 2003. A structural mechanics approach for analysis of carbon nanotubes. International Journal of Solids and Structures 40, 2487–2499.

Odega, G.M., Gates, T.S., Nicholson, L.M., Wise, K.E., 2002. Equivalent-continuum modeling of nano-structured materials. Composites Science and Technology 62, 1869–1880.

Overney, G., Zhong, W., Tomanek, M., 1993. Structural rigidity and low-frequency vibrational modes of long carbon tubules. Zeitschrift fuer Physik D: Atoms Molecules Clusters 27, 93–96.

Popov, V.N., 2004. Carbon nanotubes: properties and application. Materials Science and Engineering R 43, 61–102.

Popov, V.N., Van Doren, V.E., Balkanski, M., 2000. Elastic properties of single-walled carbon nanotubes. Physical Review B 61, 3078–3084.

Robertson, D.H., Brenner, D.W., Mintmire, J.W., 1992. Energy of nanoscale graphitic tubules. Physical Review B 45, 12592–12595.

Ru, C.Q., 2000a. Effective bending stiffness of carbon nanotubes. Physical Review B 62, 9973–9976.

Ru, C.Q., 2000b. Elastic buckling of single-walled carbon nanotube ropes under high pressure. Physical Review B 62, 10405–10408.

Ruoff, R.S., Dong, Q., Liu, W.K., 2003. Mechanical properties of carbon nanotubes: theoretical predictions and experimental measurements. Comptes Rendus Physique 4, 993–1008.

Salvetat, J.P., Briggs, G.A.D., Bonard, J.-M., Bacsa, R.R., Kulik, A.J., Stöckli, T., Burnham, N.A., Forró, L., 1999. Elastic and shear moduli of single-walled carbon nanotube ropes. Physical Review Letters 82, 944–947.

Sánchez-Portal, D., Artacho, E., Soler, J.M., 1999. Ab initio structural, elastic, and vibrational properties of carbon nanotubes. Physical Review B 59, 12678–12688.

Sunyk, R., Steinmann, P., 2003. On higher gradients in continuum-atomic modeling. International Journal of Solids and Structures 40, 6877–6896.

Tadmor, E., Ortiz, M., Phillips, R., 1996. Quasicontinuum analysis of defects in solids. Philosophy Magazine A 73, 1529–1563.

Tadmor, E.B., Smith, G.S., Bernstein, N., Kaciras, E., 1999. Mixed finite element and atomistic formulation for complex crystals. Physical Review B 59, 235–245.

Tersoff, J., 1988. New empirical approach for the structure and energy of covalent systems. Physical Review B 37, 6991–7000.

Treacy, M.M.J., Ebbesen, T.W., Gibson, J.M., 1996. Exceptionally high Young's modulus observed for individual carbon nanotubes. Nature 381, 678–680.

Van Lier, G., Van Alsenoy, C., Van Doren, V., Geerlings, P., 2000. Ab initio study of the elastic properties of single-walled carbon nanotubes and graphene. Chemical Physics Letter 326, 181–185.

Yakobson, B.I., Brabec, C.J., Bernholc, J., 1996. Nanomechanics of carbon tubes: instabilities beyond linear response. Physical Review Letters 76, 2511–2514.

Yu, M.F., Files, B.S., Arepalli, S., Ruoff, R.S., 2000a. Tensile loading of ropes of single wall carbon nanotubes and their mechanical properties. Physical Review Letters 84, 5552–5555.

Yu, M.F., Lourie, O., Dyer, M.J., Moloni, K., Kelly, T.F., Ruoff, R.S., 2000b. Strength and breaking mechanism of multiwalled carbon nanotubes under tensile load. Science 287, 637–640.

Zhang, P., Huang, Y., Gao, H., Hwang, K.C., 2002a. Fracture nucleation in single-wall carbon nanotubes under tension: a continuum analysis incorporating interatomic potentials. Journal of Applied Mechanics 69, 454–458.

Zhang, P., Huang, Y., Geubelle, P.H., Hwang, K.C., 2002b. On the continuum modeling of carbon nanotubes. Acta Mechanica Sinica 18, 528–536.

Zhang, P., Huang, Y., Geubelle, P.H., Klein, P.A., Hwang, K.C., 2002c. The elastic modulus of single-walled carbon nanotubes: a continuum analysis incorporating interatomic potentials. International Journal of Solids and Structures 39, 3893–3906.

Zhang, P., Jiang, H., Huang, Y., Geubelle, P.H., Hwang, K.C., 2004. An atomistic-based continuum theory for carbon nanotubes: analysis of fracture nucleation. Journal of the Mechanics and Physics of Solids 52, 977–998.

Zhou, G., Duan, W.H., Gu, B.L., 2001. First-principles study on morphology and mechanical properties of single-walled carbon nanotube. Chemical Physics Letters 333, 344–349.